ORIGINAL RESEARCH

Amphiphilic Janus Nanoparticles for Effective Treatment of Bacterial Pneumonia by Attenuating Inflammation and Targeted Bactericidal Capability

Xiangjun Chen*, Weiwei Li ⓘ*, Qing Fan ⓘ, Xiao Liu, Xuanxiang Zhai ⓘ, Xiaoyi Shi ⓘ, Wenting Li, Wei Hong

School of Pharmacy, Shandong Engineering Research Center of New-Type Drug Loading & Releasing Technology and Preparation, Binzhou Medical University, Yantai, Shandong, People's Republic of China

*These authors contributed equally to this work

Correspondence: Wei Hong; Wenting Li, Email hongwei_sy@bzmc.edu.cn; liwenting1003@163.com

Introduction: *Pseudomonas aeruginosa (P. aeruginosa)*-induced pneumonia is marked by considerable infiltration of inflammatory cells and biofilm formation, which causes acute and transient lung inflammation and infection. Nevertheless, the discovery of alternative preventative and therapeutic methods is essential due to the high mortality rates in clinical settings and the resistance of *P. aeruginosa* infection to multiple medications.

Purpose: In this research, we constructed amphiphilic Janus nanoparticles (JNPs, denoted as SSK1@PDA/CaP@CIP), loaded with hydrophobic SSK1, a β-galactosidase (β-gal)-activated prodrug for reducing macrophages, and hydrophilic ciprofloxacin (CIP), a classic antibiotic for treating infection. SSK1@PDA/CaP@CIP was designed to effectively attenuate inflammation, eradicate biofilms, and combat planktonic *P. aeruginosa*.

Results: As expected, SSK1@PDA/CaP@CIP was able to target the infection site and demonstrated outstanding efficacy in treating *P. aeruginosa* strain PAO1-induced pneumonia by regulating macrophage infiltration to reduce inflammation and removing planktonic bacteria and biofilms to control infection. Additionally, the primary organs did not exhibit any discernible pathological changes following treatment with SSK1@PDA/CaP@CIP, which indicates superior biocompatibility throughout the treatment course.

Discussion: In conclusion, our investigation introduced a promising approach to the treatment of pneumonia associated with PAO1.

Keywords: *Pseudomonas aeruginosa*, pneumonia, inflammatory responses, β-galactosidase (β-gal)-activated prodrug, amphiphilic Janus nanoparticles

Introduction

Bacterial pneumonia is the most prevalent type of pneumonia, which is an inflammation of the lungs caused by multiple factors.[1] *P. aeruginosa* is a major nosocomial infection that usually causes acute pneumonia. It is particularly hazardous to patients with malignancies, hematological diseases, metabolic diseases, and severe infections that necessitate ventilation, such as coronavirus 2019 infection.[2–5] Consequently, *P. aeruginosa* is a significant pathogenic bacterium causing hospital-acquired pneumonia and is related to with a high clinical mortality rate.[6,7]

P. aeruginosa-induced pneumonia can result in a series of events in the host, such as immune cell buildup, reactive oxygen species generation, cytokine release, inflammatory response activation, lipid metabolism disruption, and epigenetic factor modulation.[8–10] These events progressively cause chronic pathological deterioration of the respiratory system. Furthermore, *P. aeruginosa* has a higher ability to form biofilms, which results in long-term persistence in clinical settings. Self-produced extracellular polymeric substances (EPS) primarily form biofilms, which protect internal bacteria from environmental hazards and inhibit antibiotic penetration.[11–14] As a result, bacteria in biofilm form are more drug-resistant than planktonic cells by up to 10–1000 fold. Due to the highly resistant biofilm and intrinsic resistance, aggressive antibiotic therapy always leads to
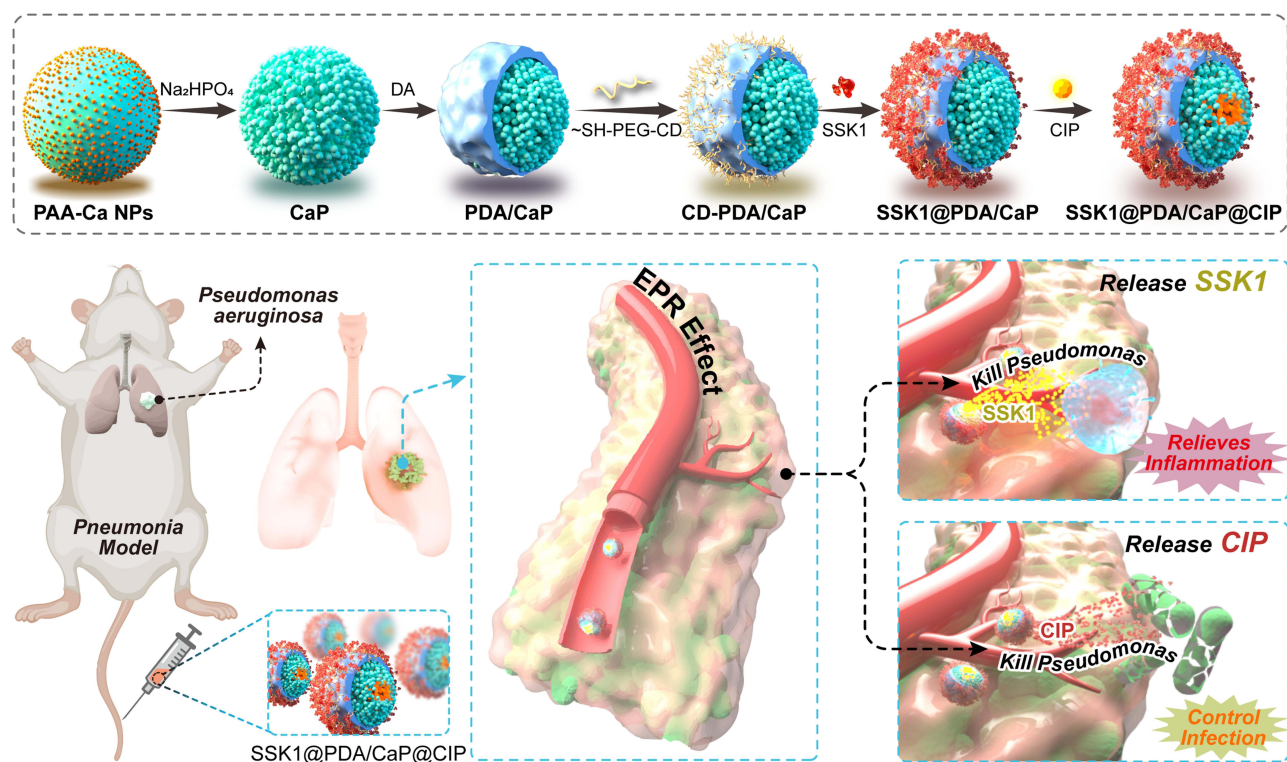
Scheme I The synthesis and schematic illustration of SSK1@PDA/CaP@CIP Janus nanoparticles for effective treatment of pneumonia by attenuating inflammation and targeted bactericidal capability.

unsatisfactory outcomes. Thus, effective therapy for *P. aeruginosa*-induced pneumonia should focus on 3 aspects: killing bacteria, eliminating biofilm, and attenuating inflammation.[15–17]

According to research, inflammatory macrophages are the primary cause of pneumonia inflammation because they release an abundant proinflammatory cytokines. Deng et al developed SSK1, a β-galactosidase (β-gal)-activated prodrug that targets macrophages. β-gal expression is a typical response to immune activation.[18] In a lung-injured animal model, SSK1 treatment effectively reduced macrophage numbers and infiltration levels, resulting in a significant alleviation in inflammation.[19]

Recently, significant attention has been paid to nanoparticle in the field of medication administration,[20–22] especially s Janus nanoparticles (JNPs).[23,24] Two distinct domains with varying chemical compositions are present in these nanoparticles, which enables the precise calibration and regulation of their properties. Independent divisions can reduce drug interactions and improve treatment efficiency. Due to its unique asymmetric design, synergistic therapy and concurrent multimodal imaging are more successful.[25]

First, we synthesized polydopamine/calcium phosphate (PDA/CaP) JNPs in our work. Mercapto-γ-cyclodextrin (CDs) were employed to decorate the bare surfaces of PDA domains and load the hydrophobic drug, SSK1. The hydrophobic interactions of CDs facilitated the encapsulation of SSK1 (designated as SSK1@PDA/CaP). The CaP sides provided storage spaces for loading hydrophilic antibiotics, ciprofloxacin (CIP, designed as SSK1@PDA/CaP@CIP). Overall, the SSK1@PDA/CaP@CIP possessed bactericidal capacity, biofilm eradication ability, and anti-inflammatory activity in a single JNP, which could act as effective nanoplatforms for the therapy of pneumonia (Scheme 1).

Materials and Methods
Materials
Detailed information on the materials that we used in the investigation was supplemented in the Supplementary Information.

Methods

Preparation of SSK1@PDA/CaP@CIP JNPs

CaP NPs Synthesis

A total of 48 mg of Ca(OH)$_2$ and 0.8 mL of PAA aqueous solution (0.2 g/mL) were added to 100 mL of DI water, and then the mixture was ultrasonically sonicated for 20 minutes to synthesized CaP. Isopropyl alcohol (IPA), 200 mL, was then gradually added while being continuously stirred. Next, the mixture was mixed with 155.2 mg of Na$_2$HPO$_4$ that had been dissolved in distilled (DI) water (500 μL). After 16 hours of constant stirring, the reaction was permitted to continue. Centrifugation was used for 8 minutes at 8000 rpm to extract the CaP NP resultant product. In order to eliminate residual impurities, the NPs were then washed three times by DI water.

PDA/CaP JNPs Synthesis

After mixing 8 mL of CaP solution with 32 mL of IPA, the pH was brought to 8–9. The reaction continued in the water bath at 32 °C for 14 hours until the solution turns blackish brown, following the addition of 9 mg of dopamine (DA). After centrifuging the PDA/CaP JNP product for 8 minutes at 9000 rpm, it was washed three times by DI water.

CD-PDA/CaP JNPs Synthesis

In this phase, 1 mg of SH-γ-CD was first dissolved in 0.1 mL of DMSO, and the PDA/CaP JNPs were pH adjusted to 10 with 2 mol/L ammonia. And 2 mL of 1 mg/mL PDA/CaP JNPs suspension (pH = 10) was gradually mixed with 1 mL SH-γ-CD solution (1 mg/mL). After 20 minutes of sonication, the mixture was reacted on a rotary mixer (11 rpm) overnight. The resulting product was centrifuged at 8000 rpm for 8 min to remove free SH-γ-CD, recovered CD-PDA /CaP JNPs, and washed with DI water.

Loading SSK1 into CD-PDA/CaP JNPs

By mixing 1 mL of SSK1 solution (0.5 mg/mL) with 3 mL of CD-PDA/CaP solution (1 mg/mL), the SSK1 loaded CD-PDA/CaP JNPs were produced. During this process, add 0.5 mg SSK1 into 0.1 mL dimethyl sulfoxide, then add 0.9 mL DI water to 1 mL. After 16 hours of continuous stirring, the mixture was centrifuged at 8000 rpm for 8 min and washed three times with DI water to remove any excess free SSK1.

Synthesis of SSK1@PDA/CaP@CIP JNPs

Briefly, 1 mL of CIP solution (1 mg/mL) and 2 mL of SSK1@PDA/CaP solution (1 mg/mL) were combined to obtain the CIP-loaded SSK1@PDA/CaP JNPs. To modify the pH to 6–7 and the volume to 1 mL, throughout this procedure, add 1 mg CIP into 0.1 mL 0.1 mol/L HCl and then 0.12 mL 0.1 mol/L NaOH. After 6 hours of continuous stirring, the mixture was centrifuged at 8000 rpm for 8 min and washed three times by DI water, in case there is any remaining free CIP. The refined SSK1@PDA/CaP@CIP JNPs were again suspended in 3 mL of DI water.

Characterization of SSK1@PDA/CaP@CIP JNPs

The particle size of the SSK1@PDA/CaP@CIP JNPs was determined using the NanoBrook 90PlusPALS analyzer (USA). The shape and surface morphology of the NPs were examined using a JEOL JEM1400 TEM (Japan). Fourier transform infrared (FTIR) spectroscopy (Nicolet IS50, USA) was used to examine the structural alterations and chemical composition of CD-PDA/CaP@CIP JNPs. The FTIR spectra of the samples varied from 4000 to 500 cm^{-1}.

CIP and SSK1 loadings in SSK1@PDA/CaP@CIP were determined by UV spectrophotometer (TU-1810, Pukin, China) and high performance liquid chromatography (LC-2050, Shimadzu, Japan), respectively. Firstly, SSK1@PDA/ CaP@CIP was centrifuged for 8 min at 8000 rpm. Next, a series of standard solutions of CIP and SSK1 with concentration gradients were established, respectively. The absorbance was measured at 276 nm with a UV-visible spectrophotometer to determine the concentration of CIP. The concentration of SSK1 was measured at 291 nm by HPLC. The chromatographic column was an Elite C18 column (250 mm × 4.6 mm, 5 μm). Mobile phase: A: water (0.01%TFA) and B: ACN (0.01%TFA). Gradient: 10% to 78% B within 48 min. Flow rate: 0.8 mL/min. The drug loading factor (DL %) of CIP and SSK1 was determined by equation (1):

$$DL\% = \frac{\text{Weight of SSK1 or CIP in Janus NPs}}{\text{Weight of Janus NPs}} \times 100\% \qquad (1)$$

The prepared SSK1@PDA/CaP@CIP was used to study the release behavior of CIP in the nanocomposite by dialysis. Briefly, the prepared SSK1@PDA/CaP@CIP was placed in a dialysis bag (MW = 3500) with 0.1 mol/L phosphate-buffered saline (PBS, pH 5.5 and 7.4) as the release medium liquid. A total of 3 mL of dialysis solution was collected and an equal volume of fresh PBS was added at scheduled time points. Cumulative CIP release was determined using UV spectroscopy, and the data were expressed as mean ± SD.

Targeted Binding of NPs Toward PAO1

Binding of Free Bacteria

The bacterial adhesion of PDA/CaP Janus NPs was assessed by incubating PAO1 suspensions with fluorescent CD-PDA /CaP@RHB, which was loaded with Rhodamine B (RHB) as a fluorescent prob. The free RHB was selected as a control. Following 0.5, 1, 2, and 4 hours of incubation, the fluorescence of RHB was assessed by an Olympus BX53F2 Fluorescent Microscope (Japan) and a BD FACSCanto II flow cytometer (USA), respectively.

Biofilm Penetration

The biofilms were created using previously approved procedures.[26,27] After that, these biofilms were treated to CD-PDA /CaP@RHB and free RHB for 0.5 hours, respectively. SYTO 9 dye was used to stain the biofilms for 30 minutes after the treatments. Zeiss LSM 880 confocal laser scanning microscopy (Germany) was used for the imaging. To acquire an all-encompassing perspective of the biofilm structure, a Z-stack imaging technique was utilized, with a 1 μm interval.

Evaluation on Antibacterial Activity

Minimum Inhibitory Concentration (MIC)

Bacterial strains were grown in Luria-Bertani (LB) medium (10 g/L tryptone, 10 g/L sodium chloride, and 5 g/L yeast extract) at 37 °C. Using the micro-dilution method, the MICs of several formulations, such as free SSK1, free CIP, SSK1/CIP combination, SSK1@PDA/CaP, PDA/CaP@CIP, and SSK1@PDA/CaP@CIP, were evaluated against PAO1 $(1 \times 10^4$ CFU/mL) at pH 5.5 and pH 7.4. Where the concentrations of CIP are 0.5, 1, 2, 4, 8, 16, 32 and 64 μg/mL, and SSK1 is the concentration in the nanoparticles corresponding to it. Bacteria suspensions served as the negative control to establish a baseline, and the measurement was performed using six independent replicate to guarantee accurate results.

Live/Dead Assay

Using a BacLight Bacterial Viability Kit, the bacterial viability of samples treated with varying pH was evaluated. These samples included free SSK1, free CIP, SSK1/CIP mixture, SSK@PDA/CaP, PDA/CaP@CIP, and SSK1@PDA/ CaP@CIP. The concentrations of SSK1 and CIP were established at 0.2 μg/mL and 1.0 μg/mL, respectively, followed by overnight incubation with PAO1 $(4\times10^8$ CFU/mL). The bacterial samples were stained after the incubation period, using a dye mixture made up of propidium iodide and SYTO 9 at a ratio of 1:1. The staining procedure was performed for 30 minutes at a steady temperature of 25 °C. Then, an Olympus BX53F2 Fluorescent Microscope (Japan) was used to take fluorescent images.

Observation with Scanning Electron Microscopy (SEM)

Through SEM examination, the effects on the bacterial suspensions caused by various formulations were further observed. PAO1 was incubated for 4 hours at 37 °C with various conditions (pH 7.4 and pH 5.5), including free SSK1, free CIP, SSK1/CIP mixture, SSK1@PDA/CaP, PDA/CaP@CIP, and SSK1@PDA/CaP@CIP. For SSK1 and CIP, the formulations employed concentrations of 0.2 μg/mL and 1.0 μg/mL, respectively, and left overnight to be treated with 2.5% glutaraldehyde. The bacterial samples were mixed and analyzed with a Zeiss EVO LS15 SEM (Germany) after the incubation period, gradually dehydrated, and coated with gold.

Janus Nanoparticles Antibiofilm Activity Evaluation

Crystal Violet Staining

Using the crystal violet staining method, the anti-biofilm efficacies of different formulations (free SSK1, free CIP, SSK1/ CIP combination, SSK1@PDA/CaP, PDA/CaP@CIP, and SSK1@PDA/CaP@CIP) in battling PAO1 biofilms were evaluated. The leftover biofilms were dyed with 0.5% crystal violet solution for 10 minutes after a 12-hour treatment. The mass of the dyed biofilms was next examined with a Japanese Olympus BX53F2 Fluorescent Microscope.

CLSM Observation

Through CLSM, the biofilm elimination capacity of SSK1@PDA/CaP@CIP was further assessed. First, free SSK1, free CIP, SSK1/CIP mixture, SSK1@PDA/CaP, PDA/CaP@CIP, and SSK1@PDA/CaP@CIP were applied to mature PAO1 biofilms during an overnight period at a concentration of 1.6 μg/mL for SSK1 or 8.0 μg/mL for CIP. Ultimately, Z-stack images were taken at 1 μm intervals using confocal laser scanning microscopy (CLSM, Zeiss LSM 880) to obtain the fluorescence images.

In vitro Cytotoxicity Against RAW264.7

The density of RAW264.7 cells was adjusted to 3×10^5 cells/mL, and the cells were seeded in 6-well plates with polylysine slides and cultured in a cell incubator overnight. The old medium was discarded and washed with PBS, and the medium containing a different preparation (free SSK1, free CIP, SSK1/CIP mixture, SSK1@PDA/CaP, PDA/ CaP@CIP and SSK1@PDA/CaP@CIP) was added, in which the concentration of SSK1 was 1.5 μg/mL, while the concentration of CIP was 7.5 μg/mL. After 4 h of incubation, the original medium was removed and washed with PBS. Calcein-AM (green fluorescence) and PI (red fluorescence) were added sequentially, and the cells were incubated at 37 °C for 20 minutes. Finally, the staining of the cells was observed by Olympus BX53F2 Fluorescent Microscope (Japan).

In vivo Targeting Study

The distribution of red fluorescent Janus nanoparticles loaded with RHB and free RHB in vivo was assessed using a well-established model of PAO1-induced biomembrane-associated lung infection. In summary, 30 μL of 4×10^6 CFU mL^{-1} bacteria were intratracheally injected into male BALB/c nude mice. After that, the mice were slowly turned vertically for 60 seconds to guarantee that PAO1 was distributed uniformly throughout the lung tissue. The mice were injected intravenously with 100 μL of free RHB and CD-PDA/CaP@RHB on the 3rd day following infection. By capturing 3D images using an IVIS spectrum in the Fluorescent Imaging Tomography mode (PerkinElmer, USA), the time-dependent biodistribution was assessed.

Pneumonia Model Determination

After intratracheally injecting 30 μL of PAO1 (4×10^6 CFU mL^{-1}), BALB/c mice were divided into 7 groups at random. On the 2nd day after infection, mice received 100 μL injections per day of 7 different preparations: (i) saline; (ii) free CIP; (iii) free SSK1; (iv) CIP/SSK1 mixture; (v) SSK1@PDA/CaP; (vi) PDA/CaP@CIP; and (vii) SSK1@PDA/ CaP@CIP. The equivalent doses of CIP and SSK1 in each NP group were 30 mg/kg and 6 mg/kg,[19] respectively. According to the experimental group, blood samples were collected from the eyeballs of mice on the 5th day after administration, and serum was collected by centrifuge tube. Serum samples were collected in centrifuge tubes and left to agglutinate for 30 min, then centrifuged for 10 min at 1000 g. Serum samples were aspirated and assayed, and the collected serum was added to microtiter plates pre-coated with antibodies to tumor necrosis factor (TNF)-α, interleukin (IL)-6, and IL-1β, and the instructions for the ELISA kit were followed. Finally, the inflammatory factor levels were detected and calculated by ELISA. Lung tissue sections were stained with F4/80 immunofluorescent staining to evaluate pulmonary infection. Every day, the mice's body weight was recorded to gaze for any possible alterations. The liver, spleen, kidney, heart, and lung were among the major organs that were removed and stained with hematoxylin and eosin (H&E) before being examined under a light microscope to check for signs of in vivo toxicity.

Statistical Analyses

The format of mean ± standard deviation (SD) was used to express the data. To compare the differences between two groups, the Student's *t*-test was employed and determined by Prism. $*P < 0.05$, $**P < 0.01$, $***P < 0.001$, and $****P < 0.0001$ denoted statistical significance.

Results and Discussions

Developing and Characterizing SSK1@PDA/CaP@CIP JNPs

Initially, PDA/CaP JNPs were generated following our earlier research.[28] The 200 nm-diameter spherical structure of the as-prepared PDA/CaP JNPs was observed (Figure 1A and B). By submerging the PDA/CaP JNPs in an acidic solution, the morphological alterations were studied using TEM and SEM, respectively, to elucidate this Janus nanostructure. Consequently, there was a significant change that resulted in the initial spherical shape changing into a PDA bowl-like arrangement (Figure 1C and D).

PDA domains were functionalized selectively with SH-γ-CD, creating PDA/CaP JNPs with hydrophobic SSK1 loading capabilities. FTIR measurements demonstrate the successful addition of SH-γ-CD (Figure 1E). Otherwise, the mean hydrodynamic diameters of PDA/CaP before (Figure S1A) and after (Figure S1B) CD modifications were measured by dynamic light scattering (DLS). A 30 nm increase in particle size proved the successful modification of CDs. The zeta potential of SSK1@PDA/CaP@CIP was around −30 mV, suggesting prolonged circulation time and good biocompatibility. The loading capability of CD-PDA/CaP was investigated by measuring SSK1 and CIP levels with HPLC and UV-Vis spectrophotometry. Based on the HPLC assay and UV-Vis spectra, CD-PDA/CaP showed a medication loading efficiency of 3.06% for SSK1 and 16.22% for CIP. SSK1@PDA/CaP@CIP JNPs released 80% of CIP after 48 hours of incubation in PBS at pH 5.5, which was much more efficient than drug release at pH 7.4 (Figure 1F). SSK1@PDA/CaP@CIP JNPs demonstrated pH-sensitive drug release activity. The breakdown of CaP in acidic conditions resulted in the accelerated release of CIP.

Bacterial Binding Affinity and Biofilm Penetration Ability

Given that NP residency time at a site of infection may be restricted, we determined how quickly NPs bind to bacteria. We studied the binding of RHB-loaded JNPs by incubating them for 0.5 to 4 hours and quantified bacteria-associated
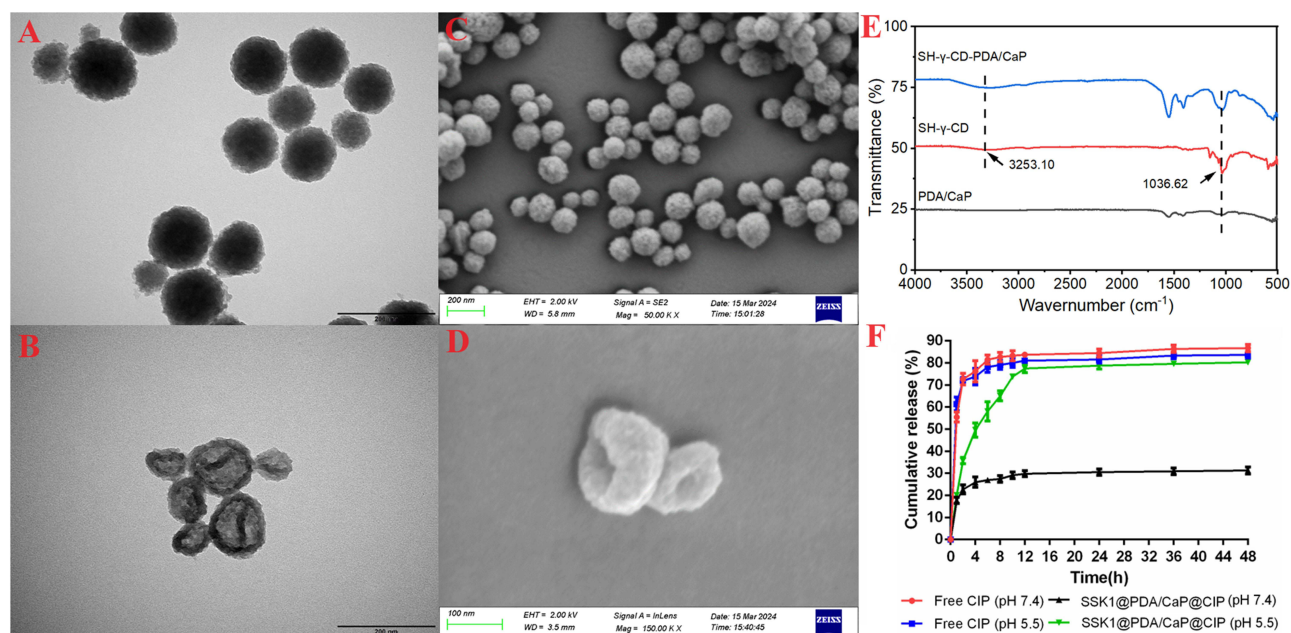

Figure 1 TEM images of PDA/CaP (**A**) and bowl-like PDA (**B**), SEM images of PDA/CaP (**C**) and bowl-like PDA (**D**), FTIR spectra of SH-γ-CD, PDA/CaP, and CD-PDA/CaP (**E**), and drug-releasing profiles of SSK1@PDA/CaP@CIP at different pH levels (**F**).

fluorescence using fluorescence microscopy and flow cytometry (fluorescence-activated cell sorting). As seen in Figure 2A, we discovered that free RHB exhibited almost undetectable red fluorescence during the incubation time, indicating that it has a low binding affinity. Fluorescent JNPs showed bright red fluorescence (Figure 2A) and rapid fluorescence saturation (Figure 2B), with approximately 80% of peak binding occurring within 0.5 hours. The binding
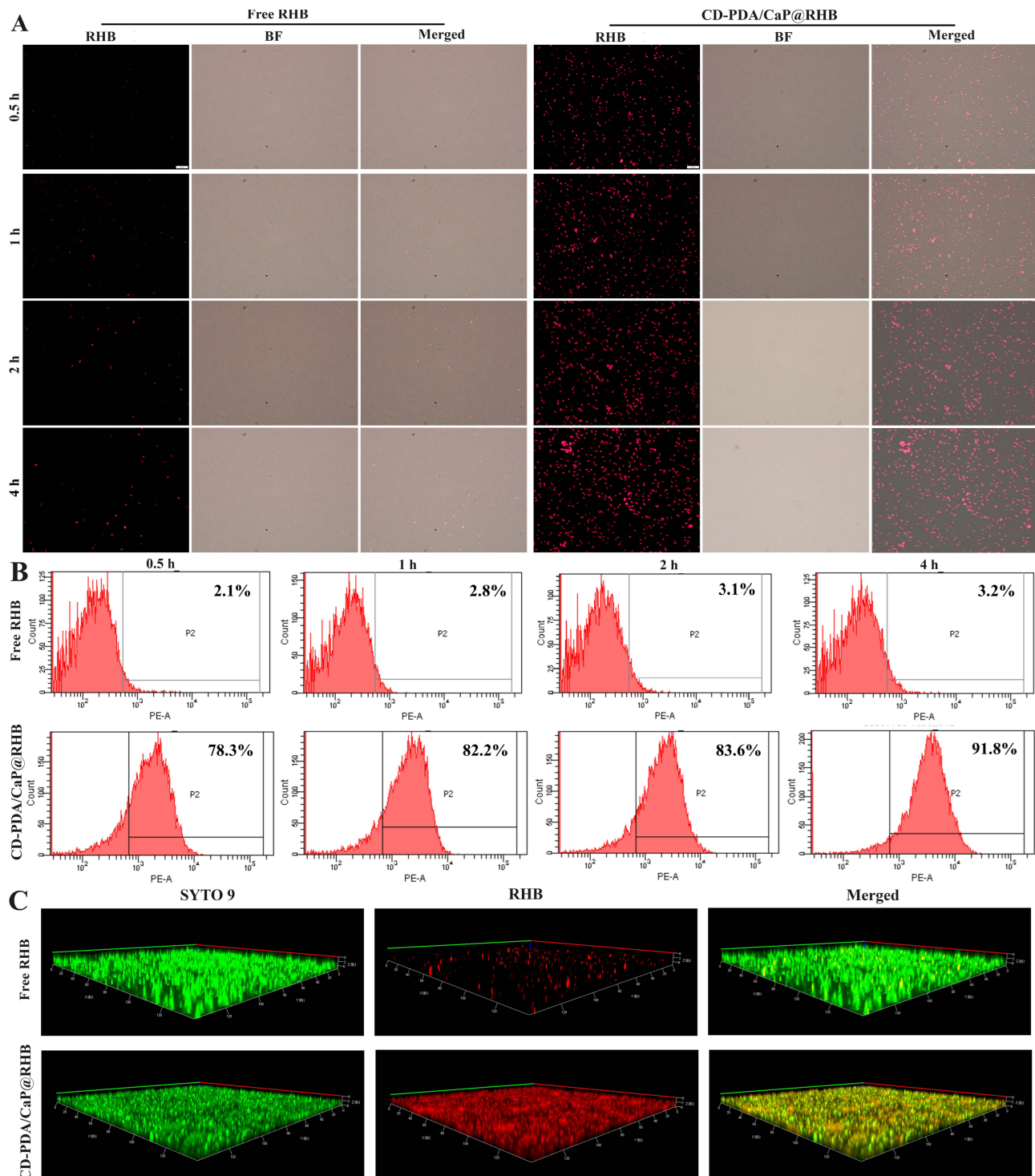

Figure 2 The bacterial binding affinity of free RHB and CD-PDA/CaP@RHB was investigated using a fluorescence microscope (**A**) and flow cytometry (**B**) after incubation for 0.5, 1 h, 2 h, and 4 hours. Scale bars=10 μm. After 0.5 hours of incubation, biofilm penetration was observed in both free RHB and CD-PDA/CaP@RHB (**C**). We have change the Figure 2 with a new one, since there is a wrong picture in the old one.

data demonstrated that PDA/CaP JNPs may adhere to bacteria with a short residence time at the infection site. The efficient bacterial binding of JNPs may be due to the adhesiveness of PDA.

The capacity to penetrate biofilms is an essential requirement for the successful removal of biofilms, as numerous diseases generate an intricate matrix consisting of extracellular polymeric substances (EPS). Thus, CLSM looked into the impact of free RHB and CD-PDA/CaP@RHB on biofilm penetration. In the naked RHB group, limited red fluorescence was shown, as seen in Figure 2C, which suggests that biofilm acts as a biological barrier against RHB. In contrast, the biofilm treated with fluorescent JNPs exhibited robust RHB signals, suggesting a high degree of penetration capability that could facilitate the delivery of loaded cargoes into the bacterial biofilms. Furthermore, after 0.5 hours of incubation, the JNPs were able to swiftly filter through the biofilm and even reach the bottom.

Bactericidal Action of SSK1@PDA/CaP@CIP JNPs in vitro

The antibacterial activities of free CIP, SSK1, SSK1/CIP mixture, SSK1@PDA/CaP, and PDA/CaP@CIP were compared with those of SSK1@PDA/CaP@CIP. Table 1 illustrates that, even at the maximum tested dose of 64 μg/mL, neither free SSK1 nor SSK1@PDA/CaP exhibited significant bactericidal activity. SSK1@PDA/CaP@CIP showed pH-dependent antibacterial activity. At pH 7.4, the MIC values of CIP-encapsulated Janus NPs were 8.0 μg/mL, which was much higher than that of free CIP. This situation might be due to the sustained release behavior of CIP at neutral condition. However, under acidic conditions (pH 5.5), SSK1@PDA/CaP@CIP exhibited comparable antibacterial activity with that of free CIP (1.0 μg/mL), which might be due to the accelerated drug release behavior. Using a Live/Dead assay, the antibacterial activity of SSK1@PDA/CaP@CIP on planktonic bacteria was further examined (Figure 3A). The concentration of CIP was set to 1.0 μg/mL. SSK1@PDA/CaP@CIP exhibited enhanced bactericidal activity under pH 5.5, as evidenced by the intense red fluorescence. It indicated that nearly all of the bacteria were killed, similar to the MIC test result. SEM was further applied to observe the morphology of *P. aeruginosa* after different treatments. As shown in Figure 3B, for SSK1 and SSK1@PDA/CaP-treated groups, *P. aeruginosa* kept their characteristic shapes, and no obvious disruption was observed on the surface of the bacteria. When the cells were treated with CIP-loaded formulations, microbial deformations, and damaged surfaces were observed.

Biofilm Eradication Assay

The ability of various treatments to eradicate biofilms was then tested using crystal violet staining. As presented in Figure 4A, all of the tested groups except the CIP-loaded NPs showed modest anti-biofilm activity. These therapies are ineffectual because free CIP has low biofilm penetration and SSK1 has a minimal sterilizing action. PDA/CaP@CIP and SSK1@PDA/CaP@CIP demonstrated effective sterilization and anti-biofilm activities, with CIP-treated NPs becoming lighter at concentrations over 8.0 μg/mL. Furthermore, CLSM showed that different formulations shared similar anti-biofilm characteristics (Figure 4B). After co-culturing PDA/CaP@CIP and SSK1@PDA/CaP@CIP, Live/Dead staining revealed that biofilms were severely destroyed and dead bacteria were dramatically increased (red fluorescence).

Table 1 MIC Values of Tested Formulations Against P. aeruginosa Under Various pH Levels

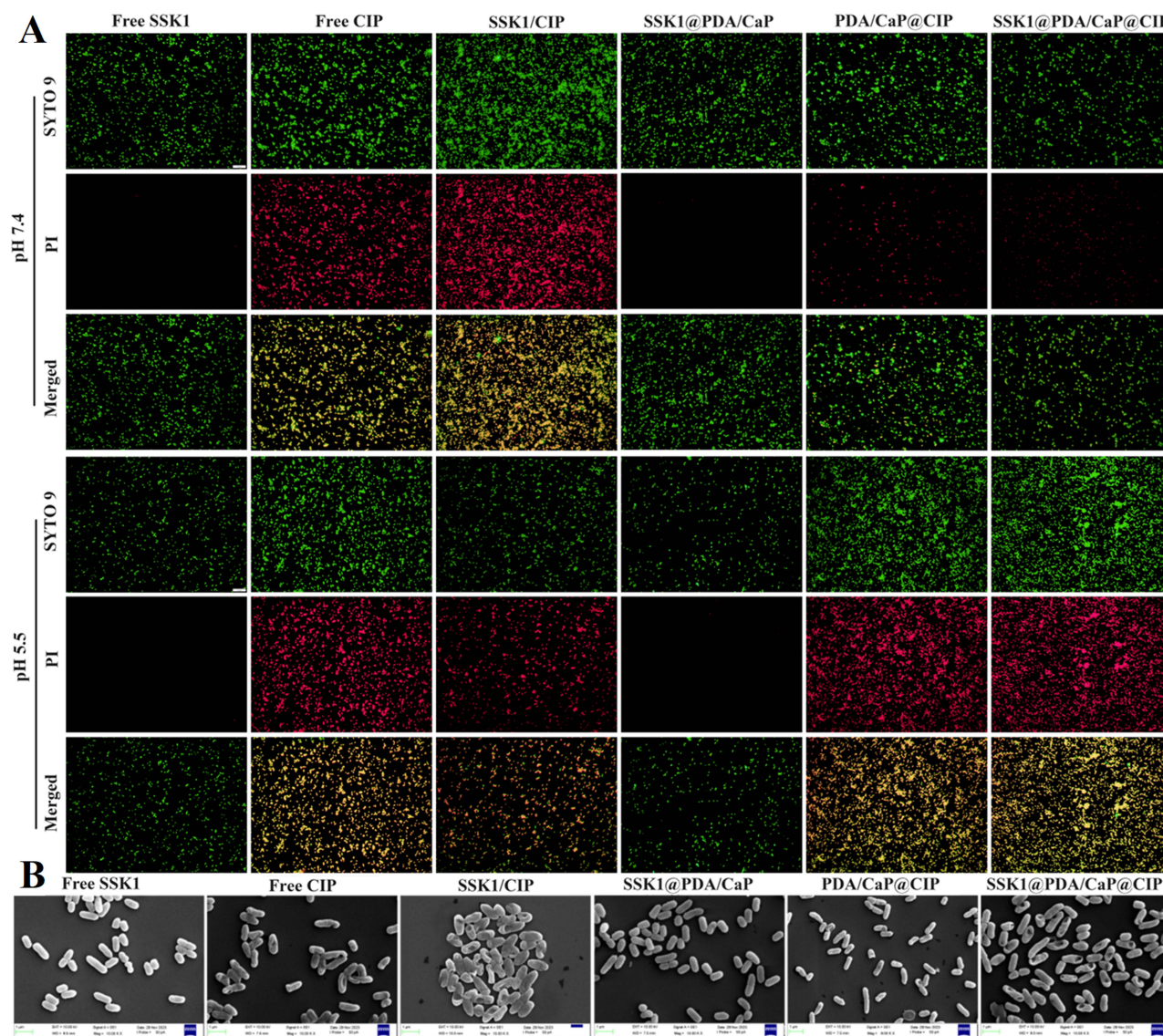| Formulations	MIC (μg/mL)	
	pH 7.4	pH 5.5
Free SSK1	> 13	> 13
Free CIP	1.0	1.0
SSK1/CIP	1.0	1.0
SSK1@PDA/CaP	> 64	> 64
PDA/CaP@CIP	8.0	1.0
SSK1@PDA/CaP@CIP	8.0	1.0

Figure 3 Live/Dead assay of *P. aeruginosa* following treatment with free SSK1, free CIP, SSK1/CIP, SSK1@PDA/CaP, PDA/CaP@CIP, and SSK1@PDA/CaP@CIP at pH 7.4 and 5.5, respectively. Scale bars=10 μm (**A**). SEM images of *P. aeruginosa* following treatment with various formulations (free SSK1, free CIP, SSK1/CIP, SSK1@PDA/CaP, PDA/CaP@CIP, and SSK1@PDA/CaP@CIP) at pH 5.5 (**B**).

Cytotoxicity Against RAW264.7

SSK1, a prodrug, stimulates β-galactosidase and targets macrophages. β-gal expression is a typical physiological response to immune stimuli. SSK1 treatment effectively reduced macrophage numbers and infiltration in a lung-injured animal model, leading to significant inflammation reduction. Based on these reports, a Live/Dead assay of RAW264.7 after treatment with the various tested formulations was performed. It could be noticed that SSK1 treatment significantly reduced the live numbers of macrophages characterized as green fluorescence (Figure 5). The depletion of macrophages might regulate hyperinflammation in *P. aeruginosa* infection, which will be investigated next.

In vivo Targeting and Treatment Efficacy for P. aeruginosa-Induced Lung Infection

The targeting ability of Janus NPs was investigated, and fluorescent pictures were captured using an IVIS Spectrum equipment with the fluorescence tomography algorithm (FLIT) mode, facilitating the creation of a 3D model and precise positioning of the Janus NPs in vivo. As shown in Figure 6A, the fluorescence of CD-PDA/CaP@RHB appeared in the lung within an hour of injection, peaked at 4 hours, and remained visible for more than 24 hours. Throughout the
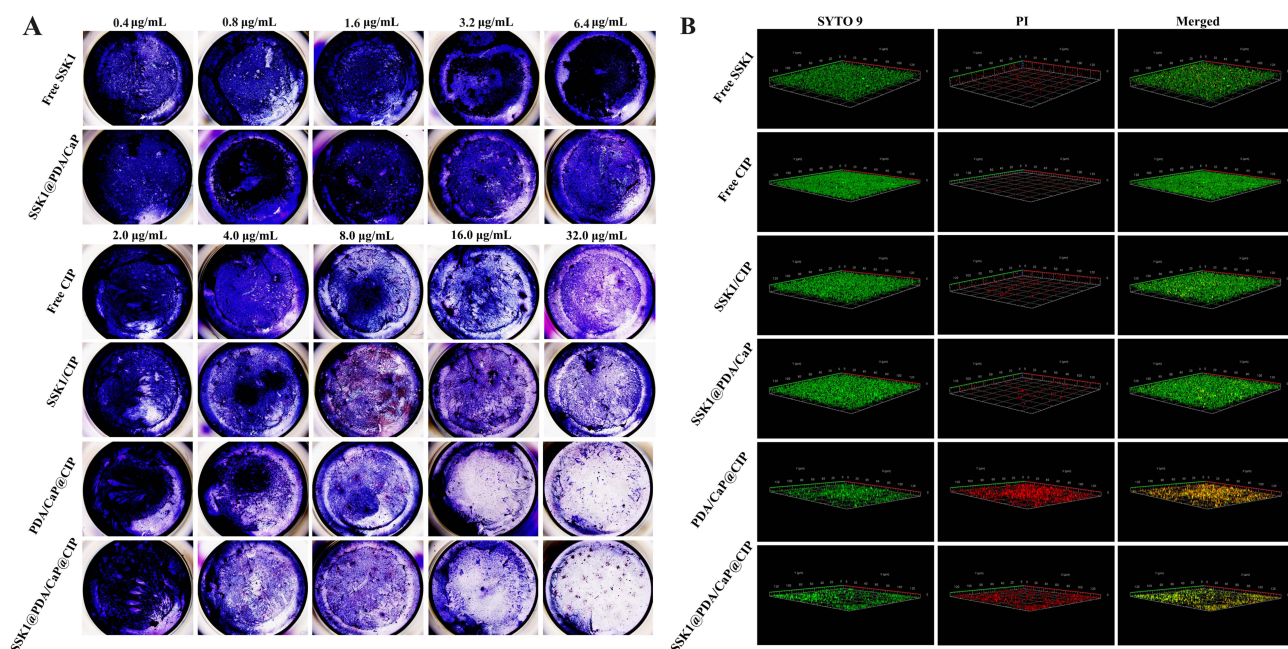
Figure 4 Biofilm imaging with crystal violet staining (**A**) and residual biofilm imaging with Live/Dead staining (**B**) after treatment with free SSK1, free CIP, SSK1/CIP, SSK1@PDA/CaP, PDA/CaP@CIP, and SSK1@PDA/CaP@CIP overnight.
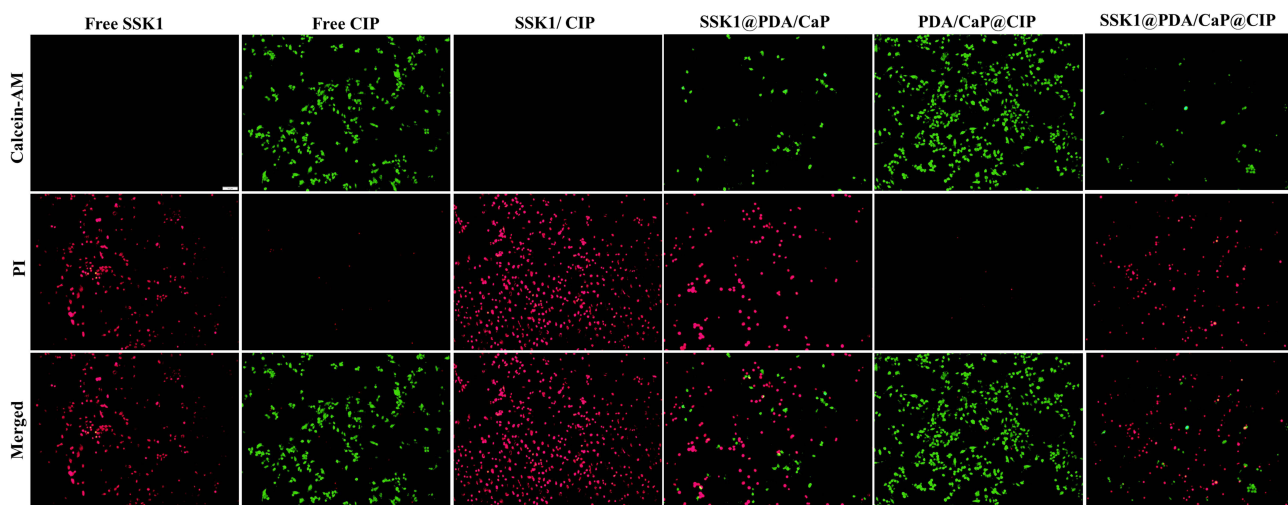

Figure 5 The Live/Dead assay of RAW264.7 after treatment with free SSK1, free CIP, SSK1/CIP, SSK1@PDA/CaP, PDA/CaP@CIP and SSK1@PDA/CaP@CIP. Scale bar=10 μm.

monitoring period, very minor fluorescence signals were detected in the infected lung following the injection of free RHB. Thus, Janus NPs may increase the target accumulation of encapsulated medicine in the lung. Furthermore, the mice were murdered at the end of the experiment, and their lungs were harvested for ex vivo fluorescence imaging. Similarly, the CD-PDA/CaP@RHB-treated group's lungs fluoresced substantially more than those treated with free RHB.

Next, since nanoparticles are typically metabolized through the kidneys, thus the in vitro cytotoxicity of SSK1@PDA/CaP@CIP against Vero cells was conducted before in vivo treatment. In addition, the potential damage of SSK1@PDA/CaP@CIP to blood cells was also determined by hemolysis assay. As shown in Figure S2, over 85% of Vero cells remained alive at the concentration of 256 μg/mL, a percentage markedly exceeding that required at clinical doses. In addition, no obvious hemolytic behavior (<5%) was observed even at the highest tested concentration. These results suggest that SSK1@PDA/CaP@CIP is well-suited for systemic administration.
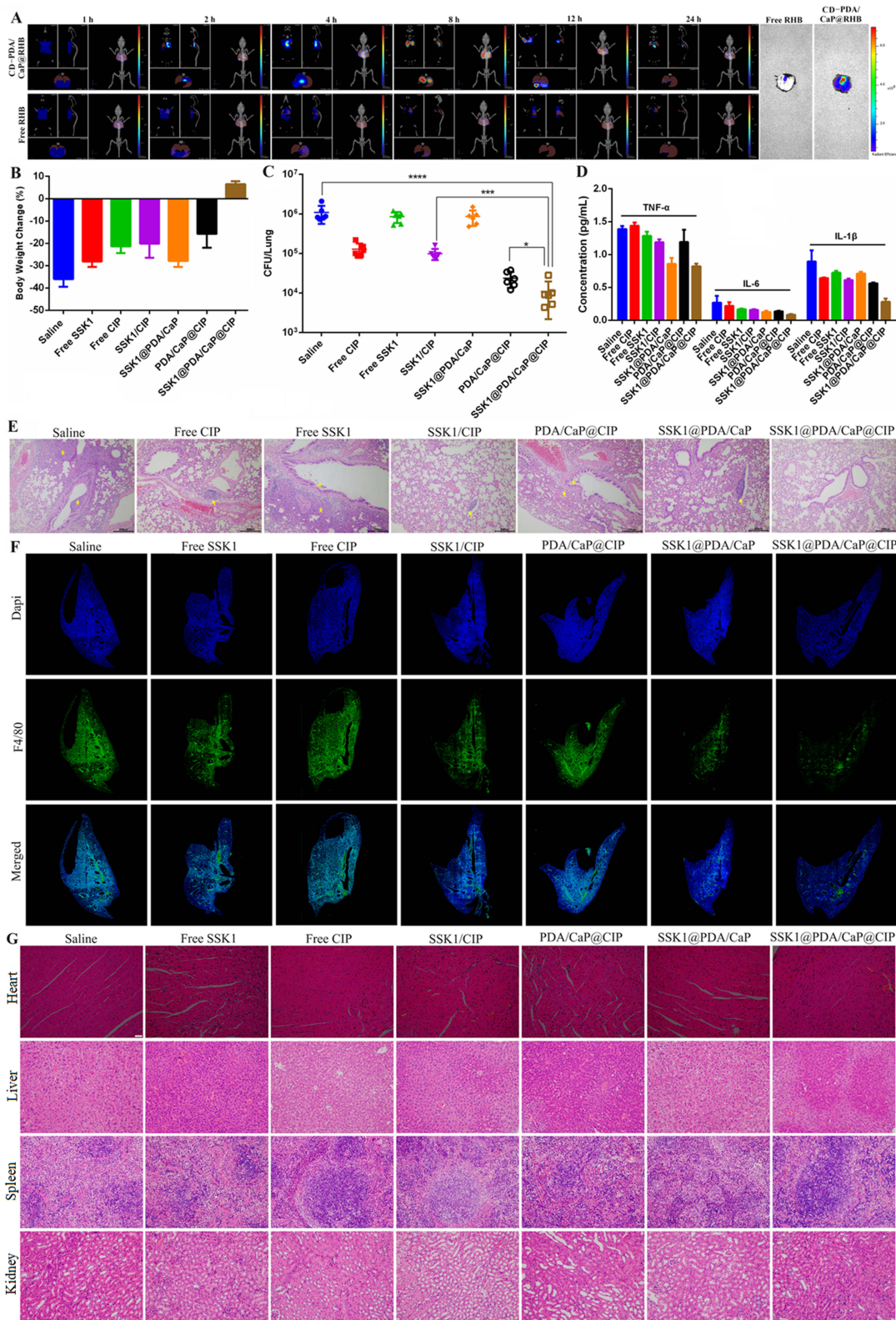
Figure 6 Fluorescent imaging of pneumonia BALB/c nude mice and ex vivo major organs after injection with CD-PDA/CaP@RHB and free RHB at different intervals (**A**). Body weight change (**B**), CFU number in lung (**C**), concentration change of inflammatory cytokines in serum samples (**D**), H&E staining of lung (**E**), immunofluorescence images of lung (**F**) and H&E staining of major organs (**G**) in pneumonia BALB/c mice after treatment with saline, free SSK1, free CIP, SSK1/CIP, SSK1@PDA/CaP, PDA/CaP@CIP and SSK1@PDA/CaP@CIP. It should be noted that the scale bar in figure E is 200 μm and that of figure G is 20 μm. *Compared to the SSK1@PDA/CaP@CIP group (*$P < 0.05$, ***$P < 0.001$, and ****$P < 0.0001$ denoted statistical significance).

Finally, the therapeutic efficiency of free CIP, free SSK1, SSK1/CIP, SSK1@PDA/CaP, PDA/CaP@CIP, and SSK1@PDA/CaP@CIP against lung-infected BALB/c mice was evaluated. We examined clinical signs throughout the study and determined that SSK1@PDA/CaP@CIP effectively prevented body weight loss, whereas saline-treated mice lost up to 30% (Figure 6B). We examined additional lung injury in mice. The mice were euthanized after taking treatment once a day for five days, and the bacterial burden in their lungs was assessed. The results showed that the number of live bacteria in the lung tissue of the SSK1@PDA/CaP@CIP group decreased dramatically, indicating high antibacterial activity (Figure 6C). We evaluated blood levels of IL-6, IL-1β, and TNF-α, which are expected to play a substantial role in pneumonia progression, after treatment. The levels of inflammatory cytokines were significantly lower in SSK1@PDA/CaP@CIP-treated animals compared to the negative control group, indicating inflammation reduction (Figure 6D).

The morphological characteristics of tissue and inflammatory cell infiltration were disclosed by H&E staining. The results indicated that SSK1@PDA/CaP@CIP significantly reduced pulmonary edema, congestion, and injury, while also enhancing pathologic changes (Figure 6E). We then examined macrophage infiltration using immunofluorescence labeling with the macrophage marker FITC Anti-F4/80 antibody. After infection, saline-treated mice exhibited a high density of F4/80-positive cells in the alveolar interstitium but only a small number in the alveoli, suggesting macrophage infiltration and activation. SSK1 treatment may prevent macrophage infiltration, especially when encapsulated in PDA/CaP Janus NPs with CIP (Figure 6F). Ultimately, after therapy with SSK1@PDA/CaP@CIP, no explicit pathological changes were found in the major organs, indicating that the molecule is biocompatible during treatment (Figure 6G). These results imply that SSK1@PDA/CaP@CIP protects against the pathological damage produced by *P. aeruginosa*-induced pneumonia.

Conclusions

To effectively treat pneumonia, SSK1@PDA/CaP@CIP, a novel nanosystem was created successfully. It combines the synergistic effects of suppressing inflammation (SSK1) and controlling infection (CIP). The SSK1@PDA/CaP@CIP JNPs exhibit efficient accumulation and outstanding adhesive properties toward the infection site owing to the nanoscale properties and PDA component. Our findings indicated that SSK1@PDA/CaP@CIP effectively mitigates pneumonic inflammation caused by *P. aeruginosa* by eliminating biofilms, killing planktonic bacteria, and depleting macrophages. This study offers valuable evidence supporting the use of SSK1@PDA/CaP@CIP in the treatment of *P. aeruginosa*-induced pneumonia.

Ethics Approval and Consent to Participate

All procedures involving animals were conducted in compliance with the Guidelines for the Care and Use of Laboratory Animals at Binzhou Medical University and were approved by the Animal Ethics Committee of Binzhou Medical University.

Funding

Disclosure

This research was conducted without any financial or inappropriate influence from other professional or personal interests.

References

1. Torres A, Cilloniz C, Niederman MS, et al. Pneumonia. *Nat Rev Dis Primers*. 2021;7(1):25. doi:10.1038/s41572-021-00259-0
2. Qin S, Xiao W, Zhou C, et al. Pseudomonas aeruginosa: pathogenesis, virulence factors, antibiotic resistance, interaction with host, technology advances and emerging therapeutics. *Signal Transduct Target Ther*. 2022;7(1):199. doi:10.1038/s41392-022-01056-1

3. Jones RN. Microbial etiologies of hospital-acquired bacterial pneumonia and ventilator-associated bacterial pneumonia. *Clin Infect Dis*. 2010;51 Suppl 1:S81–S87. doi:10.1086/653053

4. Reynolds D, Kollef M. The epidemiology and pathogenesis and treatment of Pseudomonas aeruginosa infections: an update. *Drugs*. 2021;81 (18):2117–2131. doi:10.1007/s40265-021-01635-6

5. Westblade LF, Simon MS, Satlin MJ. Bacterial coinfections in coronavirus disease 2019. *Trends Microbiol*. 2021;29(10):930–941. doi:10.1016/j. tim.2021.03.018

6. Ding C, Yang Z, Wang J, et al. Prevalence of Pseudomonas aeruginosa and antimicrobial-resistant Pseudomonas aeruginosa in patients with pneumonia in mainland China: a systematic review and meta-analysis. *Int J Infect Dis*. 2016;49:119–128. doi:10.1016/j.ijid.2016.06.014

7. Wagener BM, Hu R, Wu S, Pittet JF, Ding Q, Che P. The Role of Pseudomonas aeruginosa virulence factors in cytoskeletal dysregulation and lung barrier dysfunction. *Toxins*. 2021;13(11):776. doi:10.3390/toxins13110776

8. Thorley AJ, Grandolfo D, Lim E, Goldstraw P, Young A, Tetley TD. Innate immune responses to bacterial ligands in the peripheral human lung--role of alveolar epithelial TLR expression and signalling. *PLoS One*. 2011;6(7):e21827. doi:10.1371/journal.pone.0021827

9. Wonnenberg B, Bischoff M, Beisswenger C, et al. The role of IL-1beta in Pseudomonas aeruginosa in lung infection. *Cell Tissue Res*. 2016;364 (2):225–229. doi:10.1007/s00441-016-2387-9

10. Rada B. Interactions between neutrophils and pseudomonas aeruginosa in cystic fibrosis. *Pathogens*. 2017;6(1):10. doi:10.3390/pathogens6010010

11. Fu J, Nisbett LM, Guo Y, Boon EM. NosP detection of heme modulates Burkholderia *thailandensis* biofilm formation. *Biochemistry*. 2023;62 (16):2426–2441. doi:10.1021/acs.biochem.3c00187

12. Hu X, Li Y, Piao Y, et al. Two-tailed dynamic covalent amphiphile combats bacterial biofilms. *Adv Mater*. 2023;35(33):e2301623. doi:10.1002/adma.202301623

13. Kong Q, Qi M, Li W, et al. A Novel Z-scheme heterostructured Bi(2) S(3) /Cu-TCPP nanocomposite with synergistically enhanced therapeutics against bacterial biofilm infections in periodontitis. *Small*. 2023;19(43):e2302547. doi:10.1002/smll.202302547

14. Chen Y, Gao Y, Chen Y, et al. Nanomaterials-based photothermal therapy and its potentials in antibacterial treatment. *J Control Release*. 2020;328:251–262. doi:10.1016/j.jconrel.2020.08.055

15. Pang Z, Raudonis R, Glick BR, Lin TJ, Cheng Z. Antibiotic resistance in Pseudomonas aeruginosa: mechanisms and alternative therapeutic strategies. *Biotechnol Adv*. 2019;37(1):177–192. doi:10.1016/j.biotechadv.2018.11.013

16. Botelho J, Grosso F, Peixe L. Antibiotic resistance in Pseudomonas aeruginosa - mechanisms, epidemiology and evolution. *Drug Resist Updat*. 2019;44:100640. doi:10.1016/j.drup.2019.07.002

17. Ahmadi TS, Behrouz B, Mousavi Gargari SL. Polyclonal anti-whole cell IgY passive immunotherapy shields against P. aeruginosa-induced acute pneumonia and burn wound infections in murine models. *Sci Rep*. 2024;14(1):405. doi:10.1038/s41598-023-50859-x

18. Cai Y, Zhou H, Zhu Y, et al. Elimination of senescent cells by beta-galactosidase-targeted prodrug attenuates inflammation and restores physical function in aged mice. *Cell Res*. 2020;30(7):574–589. doi:10.1038/s41422-020-0314-9

19. Lu S, Zhao J, Dong J, et al. Effective treatment of SARS-CoV-2-infected rhesus macaques by attenuating inflammation. *Cell Res*. 2021;31 (2):229–232. doi:10.1038/s41422-020-00414-4

20. Mosallam FM, Elshimy R. Eradication of Klebsiella pneumoniae pulmonary infection by silver oxytetracycline nano-structure. *AMB Express*. 2024;14(1):62. doi:10.1186/s13568-024-01720-5

21. Gomaa SE, Shaker GH, Mosallam FM, Abbas HA. Knocking down Pseudomonas aeruginosa virulence by oral hypoglycemic metformin nano emulsion. *World J Microbiol Biotechnol*. 2022;38(7):119. doi:10.1007/s11274-022-03302-8

22. Mosallam FM, Abbas HA, Shaker GH, Gomaa SE. Alleviating the virulence of Pseudomonas aeruginosa and Staphylococcus aureus by ascorbic acid nanoemulsion. *Res Microbiol*. 2023;174(7):104084. doi:10.1016/j.resmic.2023.104084

23. Huang Y, Liu D, Guo R, Wang B, Lu Y. Intelligent jellyfish-type janus nanoreactor targeting synergistic treatment of bacterial infections. *ACS Appl Bio Mater*. 2023;6(6):2384–2393. doi:10.1021/acsabm.3c00204

24. Fan X, Yang J, Loh XJ, Li Z. Polymeric janus nanoparticles: recent advances in synthetic strategies. *Materials Properties, and Applications, Macromol Rapid Commun*. 2019;40(5):e1800203. doi:10.1002/marc.201800203

25. Zhang MJ, Zhang LY, Chen YD, Li L, Su ZM, Wang CG. Precise synthesis of unique polydopamine/mesoporous calcium phosphate hollow Janus nanoparticles for imaging-guided chemo-photothermal synergistic therapy. *Chem Sci*. 2017;8(12):8067–8077. doi:10.1039/C7SC03521G

26. Su L, Li Y, Tian S, et al. Synergy between pH- and hypoxia-responsiveness in antibiotic-loaded micelles for eradicating mature, infectious biofilms. *Acta Biomater*. 2022;154:559–571. doi:10.1016/j.actbio.2022.10.020

27. Petraitiene R, Petraitis V, Zaw MH, et al. Combination of systemic and lock-therapies with micafungin eradicate catheter-based biofilms and infections caused by candida albicans and Candida parapsilosis in neutropenic rabbit models. *J Fungi*. 2024;10(4):293. doi:10.3390/jof10040293

28. Chen X, Fan Q, Li K, et al. Amphiphilic Janus nanoparticles for nitric oxide synergistic photodynamic eradication of MRSA biofilms. *Biomater Sci*. 2024;12(4):964–977. doi:10.1039/D3BM01510F